GESS

GLOBAL.EARTHQUAKE.SATELLITE.SYSTEM

A 20-YEAR PLAN TO ENABLE EARTHQUAKE PREDICTION

MARCH 2003

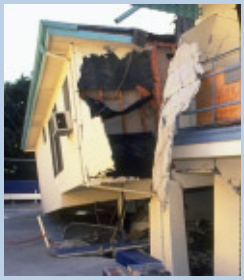

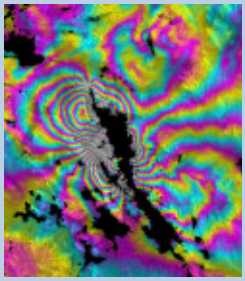

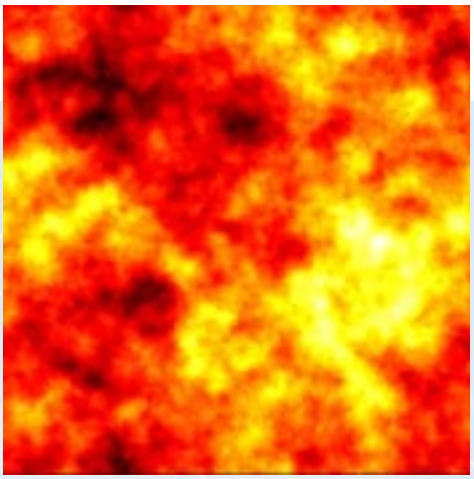

Optimizing the Measurement

CHAPTER FIVE

Measuring surface deformation from space at the required accuracy and frequency for earthquake studies constitutes numerous challenges. Methods to improve the measurement capabilities presented in this report include the possibility of using a medium Earth orbit (MEO), and developing ways to reduce the noise from atmospheric effects.

Inset: Simulated tropospheric delay. Background: Orbit path and footprint from a MEO spacecraft for GESS.

Spectrum of Options: LEO+, MEO, GEO

The mission concepts explored in this study constitute the extremes of a range of options for a global earthquake-monitoring satellite system. The LEO and LEO+ concepts, which have many similarities, are near-term possibilities that entail the use of conventional technology in mission architectures akin to those of existing SAR spacecraft. On the other hand, the geosynchronous concept is an ambitious, far-term possibility that would be dramatically different from any current SAR system in terms of its technology, operation, and performance. A middle ground may be possible, and in fact potentially desirable.

The main differences between the LEO/LEO+ concepts and the geosynchronous concept arise from the disparity in the satellite orbital altitudes — around 1000 km for the LEO/LEO+ cases vs. 35,800 km for the geosynchronous case. Higher-altitude orbits place more demanding requirements on the radar instrument: Considerably more power is required, as well as a physically larger radar antenna in order to maintain acceptable range-Doppler ambiguity performance. At the same time, higher orbits also provide more comprehensive Earth coverage as well. Although a sensor's area coverage rate for fixed resolution is limited by range-Doppler ambiguities and is consequently independent of altitude, a higher-altitude sensor would generally have land areas of interest in view more often, so the effective or "useful" coverage rate would be greater for higher-altitude sensors. A SAR constellation at MEO (between around the LEO and GEO altitudes) might strike a good balance between instrument complexity and Earth coverage.

Under the assumption that the SAR visible-swath width is limited by the ground-incidence angle, the visible-swath width increases with altitude, as depicted in Figure 5.1. Points are marked on these curves at altitudes

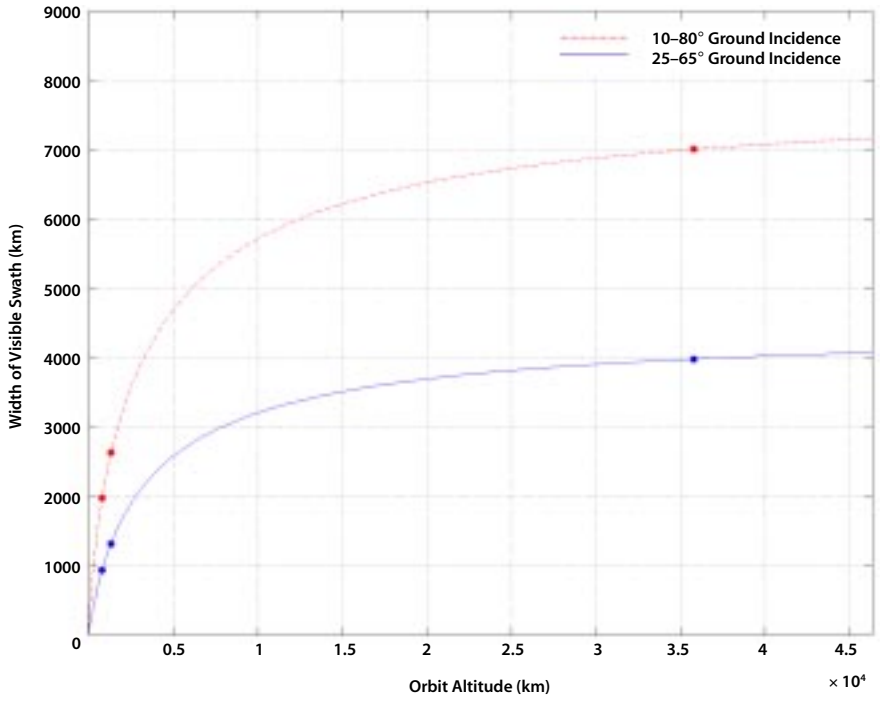

Figure 5.1
Plots of one-sided SAR swath width for different ground incidence angle limits as a function of platform altitude. Markers are for LEO, LEO+, and GEO satellites.

corresponding to the LEO (800 km), LEO+ (1325 km), and geosynchronous (35,800 km) concepts. As the altitude increases towards infinity, the visible-swath width approaches an asymptotic limit determined by the curvature of the Earth. An incremental change in orbit altitude thus has a much greater impact on the swath width at lower altitudes than at higher ones.

Considering broadside image acquisitions only, a crude estimate of a SAR platform's two-sided daily coverage area might be computed by multiplying the two-sided visible swath widths of Figure 5.1 by the average nadir velocity of the spacecraft and integrating over one day. Plots of such estimates are shown in Figure 5.2. (Note that ground areas can come into view several times per day, so the coverage area plotted can be larger than the total surface area of the Earth.) Because the nadir velocity decreases with altitude while the swath width increases, these curves peak at MEO altitudes. Such estimates of the daily coverage area are somewhat oversimplified, however. These estimates do not account for areas accessible through squinted acquisition geometries (see Figure 5.3), and the finite along-track footprint widths of high-altitude sensors can have a dramatic effect on Earth coverage. The estimates also do not account for the ground-track curvature typical of high-altitude orbits, nor do they account for the fact that high-altitude orbits might be more easily designed for better coverage of particular target areas. Furthermore, it may be more difficult to obtain two-sided coverage from lower altitudes since doing so would likely require mechanical rather than electronic antenna beam steering. These factors imply that, in practice, the effective peaks in daily coverage might occur at MEO altitudes somewhat higher than shown in Figure 5.2. More detailed system trade analyses and cost studies

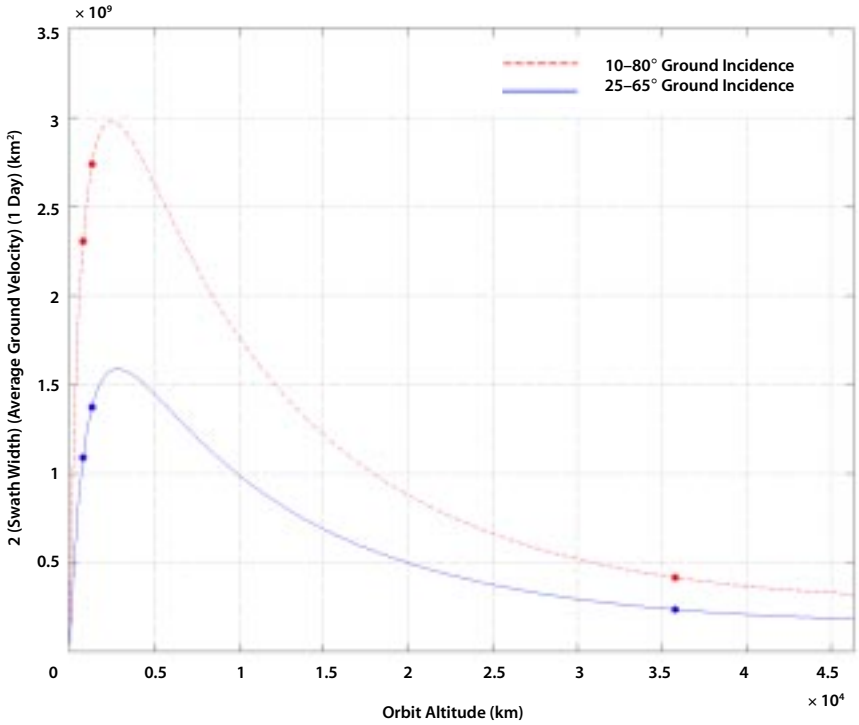

Figure 5.2
Two-sided daily broadside coverage area as a function of platform altitude assuming broadside acquisitions only. The locations of the peaks will be at higher MEO altitudes if other factors are considered. Markers are for LEO, LEO+, and GEO satellites.

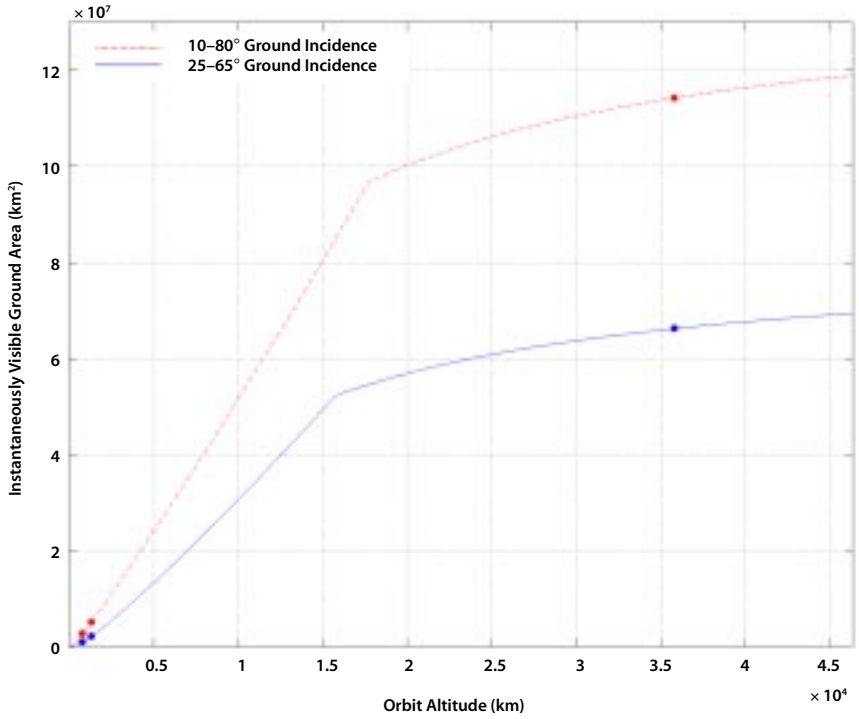

Figure 5.3
Two-sided instantaneous accessibility. Area of the sensor two-sided visible footprint as a function of platform altitude. Markers are for LEO, LEO+, and GEO satellites.

would be required to determine the optimal satellite altitude given the factors described above.

Figure 5.3 is perhaps more telling of the Earth-coverage advantages of high-altitude sensors. This plot shows the two-sided instantaneously accessible area, or in other words, the area of the two-sided sensor visible footprint. For low to moderate orbital altitudes (i.e., before the break point at about 18,000 km altitude), the along-track width of the sensor footprint is limited by the maximum azimuth angle to which the radar antenna beam can be steered electronically. At higher altitudes, the along-track footprint width is limited by the squint angle on the ground. The curves shown assume up to ±15° of azimuth beam steering and up to ±60° of ground squint. For the case of the lower curve, the footprint of the geosynchronous sensor is approximately 30 times larger than that of the LEO+ sensor. On the other hand, a MEO sensor at half the altitude of the geosynchronous sensor (17,900 km) would have a footprint area 83% of the size of its geosynchronous counterpart.

Clearly, the goal of around-the-clock accessibility for quick-response imaging favors the use of higher-altitude sensors. As the satellite relative velocity decreases with altitude, however, the integration time required to form an image may become significant compared to the event-response time. The average integration time required for 10-m resolution is shown in Figure 5.4. For the geosynchronous case, the integration time could be up to several minutes. This factor would need to be accounted for in more detailed trade studies.

High-altitude SAR systems could provide extensive Earth coverage, but their associated demands on the radar hardware cannot be neglected. Figure 5.5 illustrates the relationship

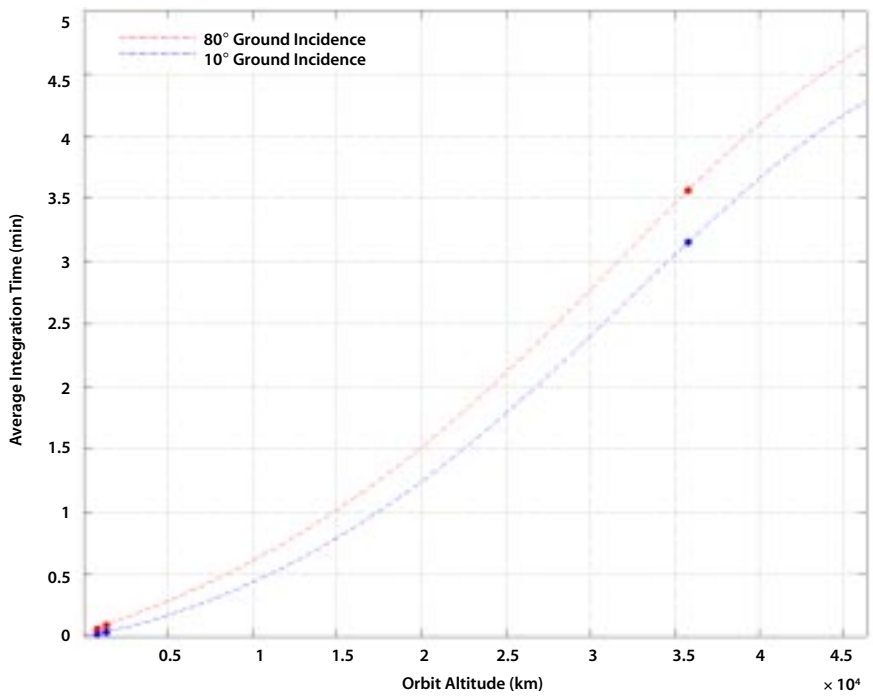

Figure 5.4
Synthetic aperture integration time required for 10-m resolution as a function of platform altitude. The required integration time can be several minutes or more at high altitudes. Markers are for LEO, LEO+, and GEO satellites.

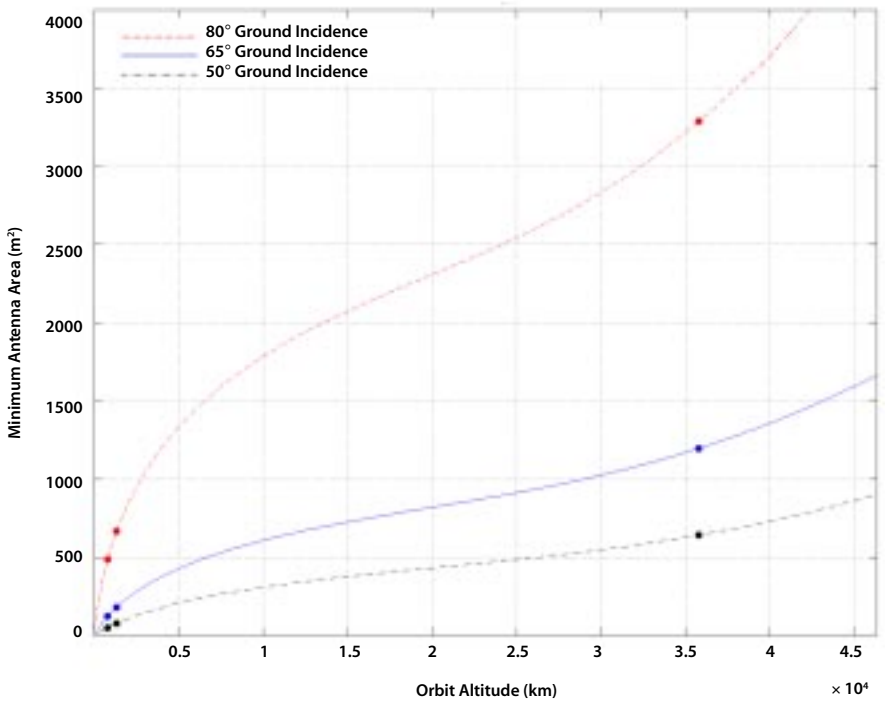

Figure 5.5
Ideal minimum antenna area as a function of platform altitude for various maximum ground incidence angles. Higher platform altitudes require larger antenna apertures. Markers are for LEO, LEO+, and GEO satellites.

between the orbital altitude and the required ideal antenna area for a number of different ground incidence angles. The required antenna area is driven by the need to avoid range-Doppler ambiguities and increases with both altitude and ground incidence angle. Higher altitudes place less-severe requirements on the electronic-steering capabilities of the radar antenna, however. Figure 5.6 depicts, as functions of altitude, the far-range look angles corresponding to two different far-range ground incidence angles. For nadir-pointed antennas, the far-range look angle is equal to the maximum elevation steering angle. From the curves shown, it is evident that electronic beam steering from side to side would be quite challenging at lower altitudes.

Although the parametric analyses presented in this section are somewhat simplified, they strongly suggest that MEO architectures deserve further consideration. A constellation of SAR sensors in MEO orbits could likely provide performance similar to that expected from a geosynchronous constellation while doing so with smaller antennas, reduced power, and lower launch costs. Space radiation at MEO altitudes is known to be rather severe, but because the specific characteristics of the radiation environment (e.g., particle energies) must also be considered in the context of the eventual system design, MEO orbits might still be ideal for future SAR missions.

Atmospheric Analysis and Mitigation

Another method for improving measurements from a GESS is to mitigate atmospheric noise effects. Because InSAR observations of surface displacement are obtained through the measurement of signal time delays, variability in the signal propagation properties of the atmosphere can seriously degrade the accuracy of the InSAR technique. If not accounted for, minute changes in the atmosphere's index of refraction can lead to data artifacts that are

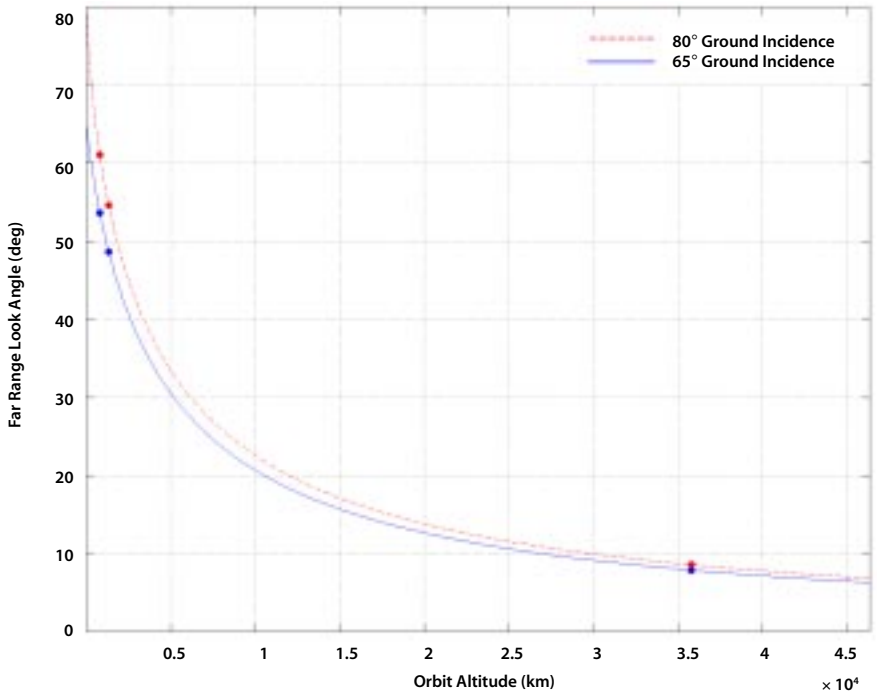

Figure 5.6
Far-range look angle as a function of platform altitude. Because of the greater variation in look angle, side-to-side electronic beam steering is more difficult from lower altitudes. Markers are for LEO, LEO+, and GEO satellites.

difficult to distinguish from true surface motion; hence, an important aspect of the GESS study has been the characterization of propagation effects introduced by the troposphere and the ionosphere. Effective signal path delays arise in both of these layers, but the mechanisms by which they occur differ. Different mitigation strategies are consequently implied. On the whole, the mitigation strategies for each are common to the LEO, LEO+, and geosynchronous cases, however.

The ionosphere is a dispersive medium and produces several frequency-dependent effects on a radar signal affecting both the resulting single-channel SAR imagery and two-channel interferometric imagery (Figure 5.7). The group delay slows down the radar pulse relative to free space, while the phase delay advances the phase relative to that of free space. The Faraday rotation alters the polarization of the return signal, although this effect is small at the planned GESS frequencies. One may take advantage of the frequency dependence of the group and phase delays to determine the magnitude of the ionospheric total electron content (TEC) and changes in the TEC over time.

Global and large-scale ionospheric fluctuations are associated with solar UV excitation, and are modulated diurnally and seasonally. These can cause propagation delays at L-band of typically 10 to 40 m, but up to 100 m and more in rare instances. Intermediate-scale disturbances (tens to hundreds of kilometers in extent) include traveling ionospheric disturbances (TIDs) and gravity waves induced by a variety of phenomena. These can alter the propagation delay by up to 5–10%. Small-scale disturbances (ionospheric "blobs" less than approximately 10 km in size) may result in scintillation or SAR defocusing, but tend to be small in magnitude. Larger magnitude small-scale structure does exist near the poles and at times along the equator, however. Total day-to-day variability can exceed a few meters of delay, or up to 25% of the total delay. To

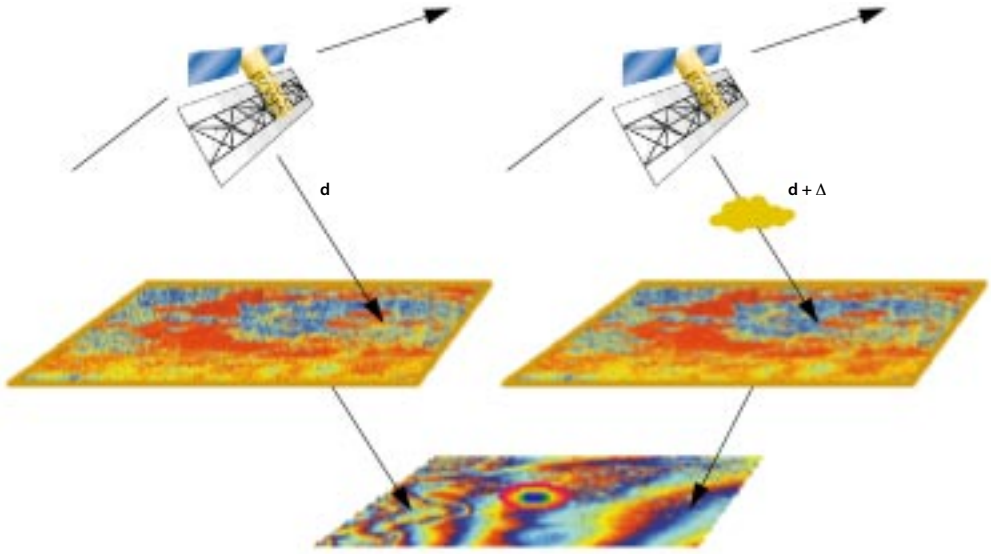

Figure 5.7
Atmospheric signal path delays that change over time create undesired artifacts in differential interferometric imagery.

observe range changes at the centimeter level, the ionospheric effects must be removed almost completely.

We have examined two dual-frequency, or split-spectrum, scenarios. In the first, we assume that GESS transmits a chirp waveform at two L-band (~1250 MHz) frequencies, each 10 MHz wide, separated by 70 MHz. In the second, we envision an additional C-band antenna transmitting a 10 MHz-wide chirp centered at 5350 MHz. We have applied concepts to interferometric SAR similar to those developed for removing ionospheric effects from GPS signals using the GPS dual frequency range and phase observables. Although there are significant differences between GPS and SAR, much work appears applicable. These dual-frequency approaches appear to be capable of removing the ionosphere at the level that GESS requires, at least for intermediate- and larger-scale ionospheric features (10 km and up).

Splitting the spectrum for a single epoch, a single pass of SAR data permits an estimate of the total ionospheric range delay measurement. The apparent range difference of identical features in the split-spectrum images is

$$\Delta\rho = \alpha T \left(\frac{1}{f_1^2} - \frac{1}{f_2^2} \right)$$

where the range offset is proportional to T, the line-of-site TEC of the ionosphere, and to the difference of the squared inverses of the two frequencies (Figure 5.8). The larger the frequency difference, the larger the effect, although for very different frequencies, the ground imagery changes significantly in other ways. By averaging the observed range offset over areas about 20 km across (depending on terrain and ground features), the total ionospheric delay may be determined to as little as 0.5 TEC units (TECU), equivalent to about 10 cm of ground displacement for differential interferometry.

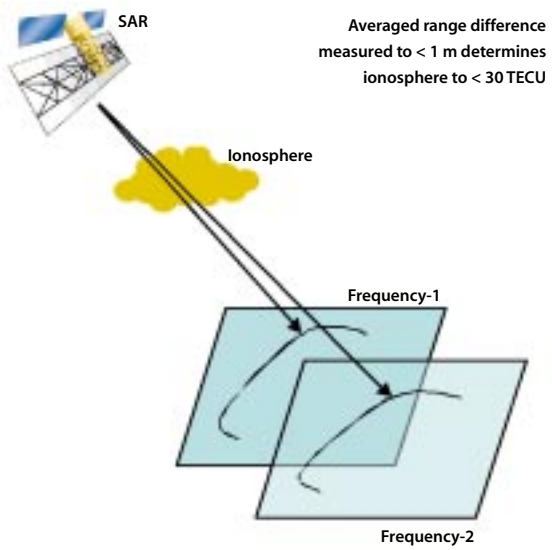

Figure 5.8
Due to the ionosphere, the range of objects in the image changes with frequency.

Splitting the spectrum for two-epoch differential interferometry yields a higher precision estimate of the change in the ionosphere between the two epochs, but no information about the total ionospheric delay. The change in scaled phase due to ionospheric effects is

$$\Delta\varphi = \alpha \Delta T \left(\frac{1}{f_1^2} - \frac{1}{f_2^2} \right)$$

where the phase difference is proportional to the change in state of the ionosphere, ΔT. By averaging the interferometric range difference over large enough areas (~10 km on a side), the change in the ionosphere at the required level (0.05 TEC units is approximately 1 cm) may be determined. Thus, intermediate-sized ionospheric perturbations can be estimated and removed from the interferometric data (Figure 5.9). Large-amplitude, smaller-scale perturbations may prove extremely difficult to remove, however.

Unlike the ionosphere, the troposphere is not dispersive, so path delays introduced by the troposphere cannot be removed through split-spectrum techniques. Rather, refractive-index variations in the troposphere stem from inhomogeneities in the air within the lowest several kilometers of the atmosphere. The associated signal-path delays are sometimes associated with meteorological phenomena such as storm systems, but can also sometimes occur in what otherwise appears to be clear air.

The total signal path delay introduced by the troposphere is often decomposed into dry and wet components, where the former arises from variations in temperature and pressure, and the latter arises from variations in water vapor content. Although most of the total delay is associated with the dry term, spatial variations in the dry delay are relatively slow compared to the size of an interferogram. Artifacts from the dry delay can therefore be removed from an interferogram using only a sparse set of calibration points. Calibration data might come from meteorological data or from locations where the true surface displacement is known, and such data could provide path-delay accuracies to the level of 1 mm or better.

The wet component of the tropospheric delay poses a much greater problem for InSAR measurements. Because the wet term is rapidly varying spatially, it is much more difficult to remove via external calibration. Spatial variations in tropospheric water vapor content are caused by the turbulent mixing of the air, and because turbulence is a random process, the variability of the wet path delay is usually characterized by statistical models. The Kolmogorov model for such processes suggests that the local spatial variability of the wet delay follows power-law behavior. In other words, the expected rms difference in path delay over two points on the Earth's surface is proportional to the distance between the points, raised to some power. Equivalently, the power spectral density of the wet delay falls off linearly when plotted on a log-log scale. The overall scale factor of the variability changes by orders of magnitude depending on time and global location, however. The wet delay is also highly variable in time, so the wet-delay artifacts between the two SAR acquisitions forming an interferogram are effectively uncorrelated.

Assuming that calibration data are obtained on some regular grid over the surface under observation, the slow spatial variations in the wet delay can be removed from the interferometric data. The wet-delay residual, composed only of the quickly varying components, causes phase artifacts in the interferogram, however. The severity of these artifacts is related to the sample spacing between calibration points through the power-law model of

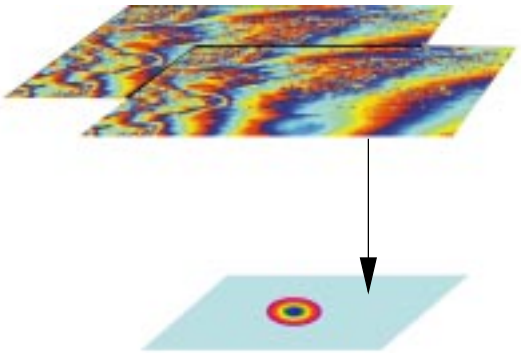

Figure 5.9
Split-spectrum interferograms combined to estimate ionosphere change.

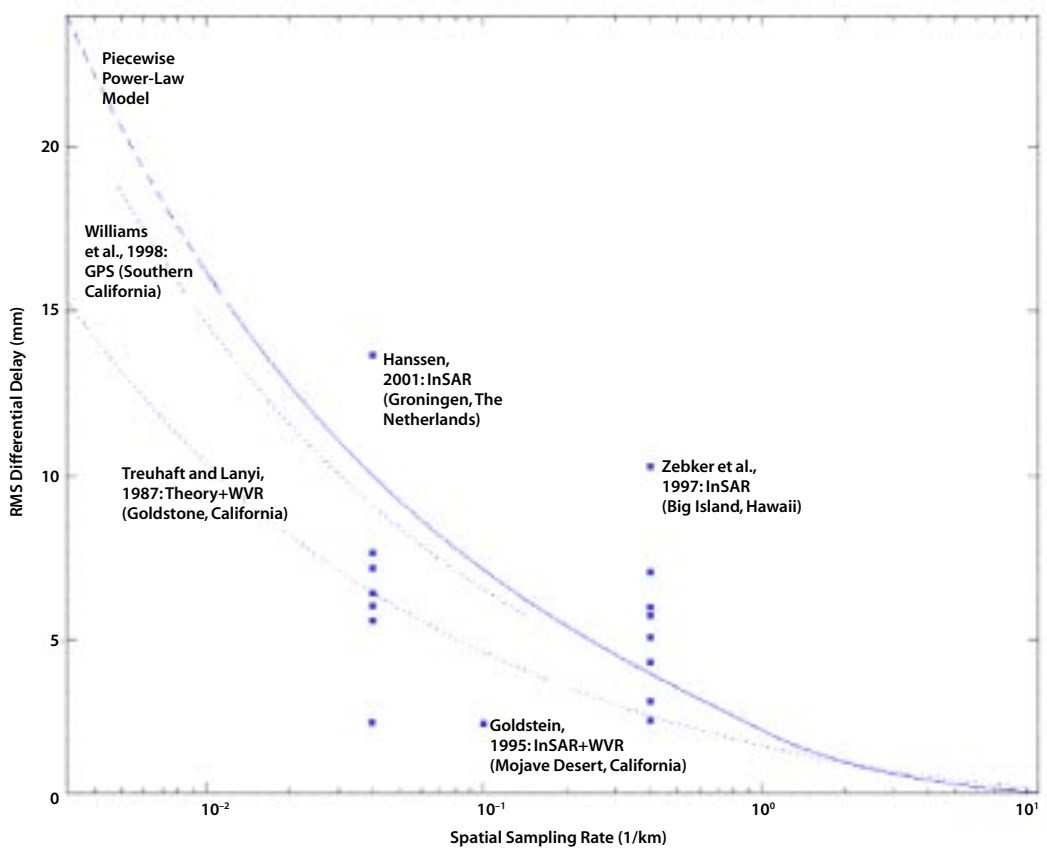

Figure 5.10
Residual one-way differential tropospheric zenith display comparing theoretical models and several data sets as calibration. The modeled residual wet tropospheric delay decreases with increased sampling rate.

the turbulence process, with artifacts becoming less severe as the grid of calibration points is made finer. Calibration data might comprise water-vapor estimates obtained from GPS or water vapor radiometer (WVR) instruments on the ground as well as downward-looking instruments on board the spacecraft. If calibration data are acquired every 10 to 100 km, the residual wet delay can be reduced to the level of 1 cm (see Figure 5.10). Calibration grids much finer than this may be impractical. Mesoscale atmospheric data assimilation models may provide data at fine resolution to correct the delay.

The residual variability in the wet delay can be further reduced through the averaging or "stacking" of multiple interferometric data sets (Sandwell and Fialko, 2002; Webb et al., 2002). Stacking reduces artifacts and noise from other sources as well, though data limitations and the desire to preserve temporal resolution imply that artifacts cannot be eliminated entirely. Advances in data-processing techniques may also offer ways of removing some tropospheric artifacts. Nevertheless, relative to other sources of error, the wet component of the tropospheric delay may prove to be a limiting factor in the accuracy of the interferometric technique if the goal is to observe millimeter-scale surface displacements. More research on this topic is required to support subcentimeter-scale displacement accuracies.

National Aeronautics and
Space Administration

Jet Propulsion Laboratory
California Institute of Technology
Pasadena, California

JPL 400-1069 03/03